Influence of Transition Metal Doping on the Structural and Electronic Behaviour of Quaternary Double Perovskite, $Cs_2AgInCl_6$, using First-Principles Calculations

To cite this article: I. B. Ogunniranye *et al* 2021 *IOP Conf. Ser.: Earth Environ. Sci.* **655** 012046

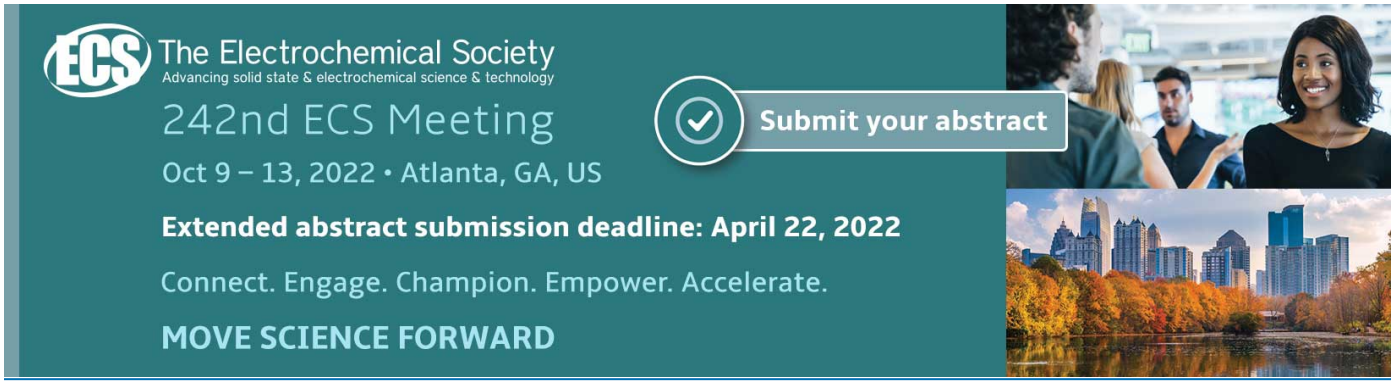

Influence of Transition Metal Doping on the Structural and Electronic Behaviour of Quaternary Double Perovskite, $Cs_2AgInCl_6$, using First-Principles Calculations

I. B. Ogunniranye[1], O. E. Oyewande[1], T. Atsue[1,2] and M. Usikalu[3]

[1] Department of Physics, Faculty of Science, University of Ibadan, Ibadan, Nigeria.
[2]Department of Physics, Faculty of Physical Science, Federal University Dutsin-Ma, Katsina, Nigeria.
[3] Department of Physics, College of Science and Technology, Covenant University, Ota, Nigeria.

ib.ogunniranye@ui.edu.ng; oe.oyewande@ui.edu.ng; tastue@fudutsinma.edu.ng

Abstract. Recently, direct bandgap double perovskites are becoming more popular among researchers in the photovoltaic community owing to their potential to address issues of lead (Pb) toxicity and structural instability inherent in lead halide (simple) perovskites. In this study, In-Ag based direct bandgap double perovskite, $Cs_2AgInCl_6$ (CAIC), is treated with transition metal doping to improve its material properties. Investigations of structural and electronic properties of Cu-doped CAIC, $Cs_2Ag_{1-x}Cu_xInCl_6$, are done using ab-initio calculations with density functional theory (DFT) and virtual crystal approximation (VCA). With the introduction of Cu-dopant, obtained results show improvement in the structural and electronic behaviour of CAIC. Based on obtained results, transition metal (Cu) doping is a viable means of treating double perovskites - by tuning their material properties suitable for an extensive range of photovoltaics, solar cells and optoelectronics.

Keywords: Virtual crystal approximation; DFT; solid solution; optimized lattice parameter; Cu-doping.

1. Introduction

Perovskite solar cells (PSCs) havegarnered much attentionas promising photovoltaic device capable of harnessing solar power effectively owing to high power conversion efficiency (PCE) of about 25.2%[1], materials availability, ease of fabrication process and low cost[2]–[8]. Methylammonium lead tri-iodide ($CH_3NH_3PbI_3$ or MAPI), atypical lead halide perovskite (LHP), is gaining popularity as an ideal light harvester and a charge carrier mediator in solar cells[3], [9], [10], because of its appealing characteristics such as;optimal direct bandgap (~1.5 eV), good photoconductivity, considerable lifetime diffusion length, high optical absorption coefficient, great bipolar transporting capability, defect tolerance ability, and low carrier effective masses with high mobility [11]–[20]. Despite these appealingqualities, MAPI still faces some fundamental issues ofinstability and toxicity associated with lead (Pb)[21]–[23], which have hindered their large scale commercialization as viable PSCs.

Substitution of toxic Pb with non-toxic elements is considered one of the viable means of resolving these issues and has subsequently led to the search for Pb-free perovskites and perovskite-derivatives materials. One way of achieving this is through direct substitution of Pb^{2+} with non-toxic group IV elements such as tin (Sn) andgermanium (Ge). Unfortunately, these produced undesirable characteristics such as poor stability and low performance of PSCs attributed to the oxidation of Ge^{2+} and Sn^{2+} to their 4+ states [24]–[26]. Another approach involves the complex substitution of Pb^{2+} wherein Pb^{2+} cation is replaced with monovalent and trivalent cations resulting in a new structure known as double perovskite (DP) [27]. DP has the general$A_2M'M''X_6$ stoichiometry, where A represents cation like Cs^+, M'denotesmonovalent cation ($M' = Ag^+$, Cu^+)and M'' trivalent cation ($M'' = In^{3+}$, Bi^{3+}), while X halides [28].

In recent times, DPs are increasingly gaining popularity among researchers in the photovoltaic research community owing to their potential to address issues of structural instability and toxicity associated with toxic lead (Pb) [28], [29]. Direct bandgap DPs are in the forefront following the pioneering work by Volonakis and co-workers in 2017 where $Cs_2AgInCl_6$ (CAIC) DP was proposed, synthesized and identified as a potential, environmentally-benign replacement for lead-based halide perovskites for applications in photovoltaic, solar cells and optoelectronics[30].CAIC is a direct-bandgap DP with high thermal and mechanical stabilities, which crystallizes in the face-centred cubic structure with space group $Fm\bar{3}m$, and has an experimental lattice parameter of 10.469 – 10.481 Å and bandgap of 2.5 - 3.3 eV [30]–[32]. However, pure bulk CAIC crystal or powder are characterized with low photoluminescence quantum yield (PLQY) and photo-absorption coefficient compared to CAIC nanocrystals and these are as a result of parity-induced forbidden transition [31], [33], [34].

Experimental findings have shown doping engineering as a fundamental means to enhance the electronic and optical properties of materials, thereby enabling their widespread usability beyond photovoltaic applications. Recent experimental studies of M-cation doping of CAIC with transition metals have been observed to improve the electronic, photoluminescence quantum yield (PLQY) and photo-absorption coefficients of CAIC [33], [35]. Specifically, Cu-doping has shown to be effectivein enhancing the photoluminescence and thermoelectric properties of materials[36], [37]. Several simulation studies of the dynamics of surfaces of materials at nanoscales had been performed using different simulation methods [38]–[42], which show potential fabrication methods for optoelectronic devices and panel surfaces.Theoretical studies based on DFT on M-cation doping in double perovskites are scarce.Given these, this work seeks to investigate the effect of Cu-doping on the structural and electronic behaviour of CAIC ($Cs_2Ag_{1-x}Cu_xInCl_6$) using the virtual crystal approximation (VCA) approach within the framework of DFT. VCA is a first-principles technique in modelling disordered solid solutionsvia pseudopotential averaging [43]. Itis effective in treating disordered systems [43], [44].

2. ComputationalMethods

The electronic structures of $Cs_2Ag_{1-x}Cu_xInCl_6$ (CAIC:Cu) solid solutionswere examined using ab-initio calculation with the virtual crystal approximation (VCA) approach[45].DFT calculations were performed using Quantum ESPRESSO (QE) software package[46], [47], with

the pseudopotential plane-wave method. The generalized gradient approximation ofPerdew-Berke-Ernzerhof (GGA-PBE) exchange-correlation (XC) functional[48]was employed for geometry optimizations;van der Waals functional (vdW-DF-OB86) [49]was chosen for lattice parameter calculation and hybrid PBE0 functional [50]applied for electronic structure calculation. The virtual atoms ($Ag_{1-x} - Cu_x$) were modelled with the Optimized Norm-Conserving Vanderbilt (ONCV) pseudopotentials [51] using the VCA approach, where the mixing ratio $x$wasvaried from 0 to 1 inthe step of 0.1.For the electron-ion interaction, ONCV pseudopotentials [51]were also employed for all calculations. In these calculations, the optimized kinetic cutoff energy of 100 Ry was set for plane-wave basis set expansion. The Monkhorst-Pack special [52] k-points sampling was set as $6 \times 6 \times 6$for optimization and PBE0 band structure calculations while a denser k-points of $12 \times 12 \times 12$wereemployed for the electronic (PBE) band structure calculations. The convergence threshold was set at 10^{-10} eV, while the force on each atomwas less than 20 meV/Å after the relaxation of entire atomic positions.

3. Results and Discussion

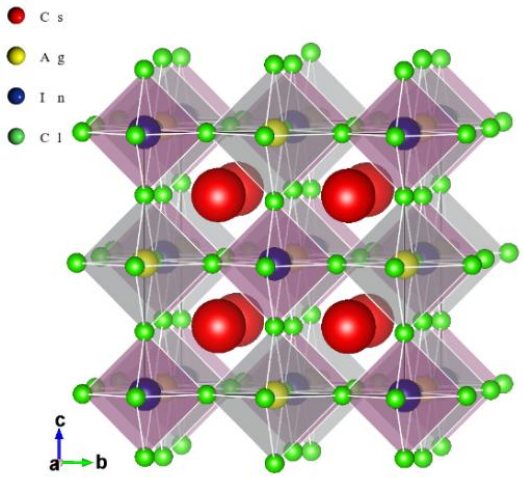

Figure 1: Polyhedral view of $Cs_2AgInCl_6$ double perovskite (space group $Fm\bar{3}m$).

The host perovskite, CAIC, crystallizes in face-centred-cubic (fcc) phase with a space group of $Fm\bar{3}m$ and its crystalline structure are illustrated in Fig. 1. Within the framework of DFT, the van der Waals functional (vdW-DF-OB86) was used to accurately describe the lattice parameter and bulk modulus of the host perovskite by using the Birch-Murnaghan [53] fit of the total energy-unit cell volume data. The calculated lattice parameter for CAIC (10.514 Å) agrees well with the experimental value (10.469)[30]. The above procedure was repeated for $Cs_2Ag_{1-x}Cu_xInCl_6$ while varying the Cu content x from 0 to 1in the step of 0.1. To ascertain the reliability of the VCA method, the lattice parameter and electronic bandgap of $Cs_2Ag_{0.5}Cu_{0.5}InCl_6$ are computed using a $2 \times 2 \times 2$ supercell. The results obtained show good agreement; 10.441 Å (10.450 Å) and 0.41 eV (0.34 eV) for VCA method (supercell alloying method).

Figures 2 and 3 show the optimized lattice parameters and bulk moduli of CAIC:Cu solid solutions. As the composition of Cu increases, the lattice parameter decreases following a linearfunction,$a(x) = 10.5128 - 0.1395x$. This function satisfies the Vegard's law for lattice parameters. Conversely, the calculated bulk modulus increases quadratically following a second-order polynomial, $B(x) = 34.0636 + 1.4576x - 0.7576x^2$. With these results, it can be inferred that the incorporation of Cu into CAIC causes the crystal lattice to shrink, thus reinforcing the material stability.

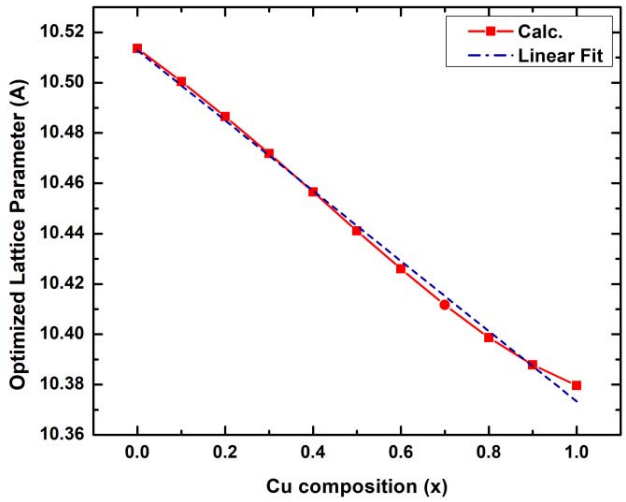

Figure 2: Calculated lattice parameters as a function of Cu composition$x$ in CAIC:Cu solid solutions, with linear fitting.

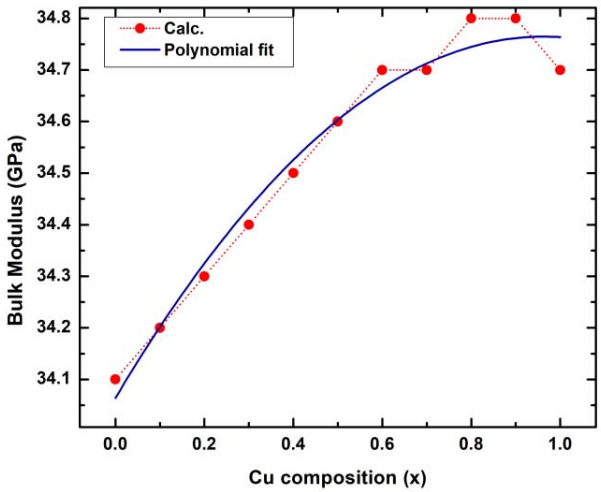

Figure 3: Bulk moduli as a function of Cu composition$x$ in CAIC:Cu solid solutions withquadratic fittings.

The electronic band structures of CAIC and CAIC:Cu solid solutions are calculated using DFT based on the first-principles calculations.At first,GGA-PBE was employedas the exchange-correlation functional for the bandgap calculation, where a bandgap underestimation of 0.95 eV

was observedwhen compared withexperimental value of 3.3 eV [30]. Table 1 shows the comparative results of the calculated bandgap with other experimental and theoretical results. To circumvent this underestimation and improve the accuracy of the bandgap, the hybrid PBE0 was used as the exchange-correlation functional where a bandgap value of 3.23 eV was obtained. The obtained result agrees well with experimental value of 3.3 eV (See Table 1).

Table 1: Calculated bandgap $\boldsymbol{E_g}$of CAIC double perovskites using different exchange-correlation functionals compared with other experimental and theoretical results.

Material		This work		Previous work	Expt.
		PBE	PBE0		
CAIC ($x = 0$)	**E_g(eV)**	0.95	3.23	2.9-3.3[30],3.33[31]	3.3[30],

The nature of bandgap, as well as the locations of conduction band maximum (CBM) and valence band minimum (VBM), can be revealed via the electronic band structure. Figure 4depicts the electronic band structure of CAIC along some selected high symmetry points, which reflect that CAIC is a directbandgap DP with both CBM and VBM located at the gamma (Γ) point in the Brillouin zone.

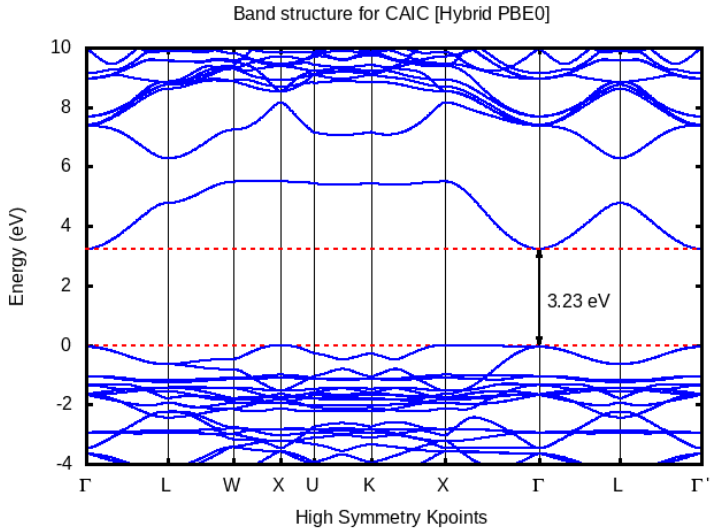

Figure 4: Electronic band structure of CAIC using PBE0 functional.

From the aforementioned above, it is worth noting that the hybrid PBE0 functional can give the most reliable bandgap value for double perovskites. With this assertion, the hybrid PBE0 functional was then used to compute the electronic band structure of CAIC:Cu solid solutions. Figure 5 shows the variation tendency in the bandgap as the Cu composition increases. By interpolating the bandgaps to a polynomial function, the bandgaps decreasequadratically with a second-order polynomial function, $E(x) = 3.2698 - 0.6463x - 0.6936x^2$, with increasing Cu content (x). This function satisfied the Vegard's law with abandgap bowing parameter,b, of -0.6936.In addition to this, the direct bandgap nature of the host perovskite remains unchanged despite the introduction of Cu-dopants. Bandgap bowing parameter (b) indicates the non-linearity of the bandgap to the composition, as well as the degree of fluctuation in the crystal

field. The results indicate enhancement in the light-harvesting ability of the materials owing to the reduction in the bandgap with increasing Cu content. Since the bandgap bowing parameter is very small, it indicates good miscibility between CAIC and CCIC ($x = 1$), and low compositional disorder.

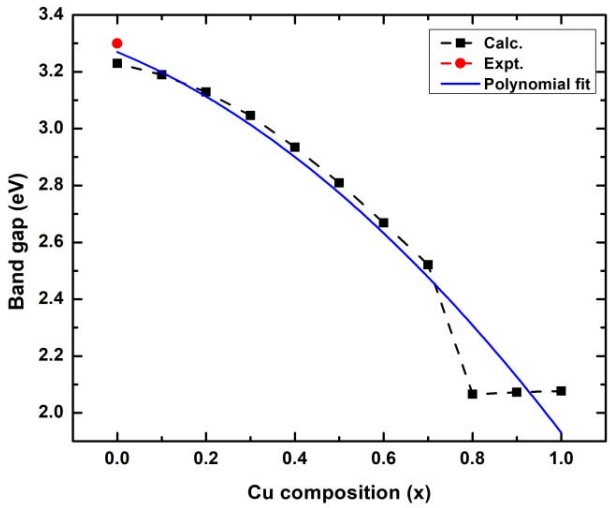

Figure 5: Calculated bandgap of CAIC:Cu solid solutions with the polynomial fit. The experiment value for CAIC is indicated with the red dot.

4. Conclusion

In this work, the effect of Cu-doping on the structural and electronic properties of CAIC has been studied using first-principles DFT calculations and VCA approach. The ab-initio VCA method was used to model the solid solutions. The PBE0 functional was used for the band structure calculations after assessing the exchange-correlation functional of GGA-PBE. With increasing Cu contents, the crystal lattice shrinks following a linear function $a(x) = 10.5128 - 0.1395x$, bulk modulus increases with a quadratic function of $B(x) = 34.0636 + 1.4576x - 0.7576x^2$, while the bandgap decreases quadratically with a second-order polynomial function, $E(x) = 3.2698 - 0.6463x - 0.6936x^2$. The variation tendencies, as a result of Cu-doping, in the structural and electronic properties of the materials under study have shown Cu to be an efficient dopant in treating double perovskites. In conclusion, $Cs_2Ag_{1-x}Cu_xInCl_6$ (CAIC:Cu) solid solutions can be presented as potential candidates for photovoltaics and optoelectronics.

Acknowledgements

The authors wish to acknowledge The Postgraduate College of the University of Ibadan, Ibadan, Nigeria for the computational access to the High-Performance Computing (HPC) resources. All the computational tasks were performed with these resources.The authors also wish to thank The Covenant University Centre for Research, Innovation and Discovery (CUCRID) for the support in publication.

References

[1] NREL, "Best Research-Cell Efficiency Chart," *National Renewable Energy Laboratory (NREL)*. 2019, Accessed: Jun. 15, 2020. [Online]. Available: http://www.nrel.gov/ncpv/images/efficiency_chart.jpg.

[2] H. J. Snaith, "Perovskites: The Emergence of a New Era for Low-Cost, High-Efficiency Solar Cells," *J. Phys. Chem. Lett.*, vol. 4, no. 21, pp. 3623–3630, Nov. 2013, doi: 10.1021/jz4020162.

[3] M. Liu, M. B. Johnston, and H. J. Snaith, "Efficient planar heterojunction perovskite solar cells by vapour deposition," *Nature*, vol. 501, no. 7467, pp. 395–398, Sep. 2013, doi: 10.1038/nature12509.

[4] J. Burschka *et al.*, "Sequential deposition as a route to high-performance perovskite-sensitized solar cells," *Nature*, vol. 499, no. 7458, pp. 316–319, Jul. 2013, doi: 10.1038/nature12340.

[5] N.-G. Park, "Organometal Perovskite Light Absorbers Toward a 20% Efficiency Low-Cost Solid-State Mesoscopic Solar Cell," *J. Phys. Chem. Lett.*, vol. 4, no. 15, pp. 2423–2429, Aug. 2013, doi: 10.1021/jz400892a.

[6] F. Di Giacomo *et al.*, "High efficiency CH3NH3PbI(3−x)Clx perovskite solar cells with poly(3-hexylthiophene) hole transport layer," *J. Power Sources*, vol. 251, pp. 152–156, Apr. 2014, doi: 10.1016/j.jpowsour.2013.11.053.

[7] S. Casaluci *et al.*, "A simple approach for the fabrication of perovskite solar cells in air," *J. Power Sources*, vol. 297, pp. 504–510, Nov. 2015, doi: 10.1016/j.jpowsour.2015.08.010.

[8] J. Liu *et al.*, "Growth and evolution of solution-processed CH3NH3PbI3-xClx layer for highly efficient planar-heterojunction perovskite solar cells," *J. Power Sources*, vol. 301, pp. 242–250, Jan. 2016, doi: 10.1016/j.jpowsour.2015.10.023.

[9] A. Kojima, K. Teshima, Y. Shirai, and T. Miyasaka, "Organometal Halide Perovskites as Visible-Light Sensitizers for Photovoltaic Cells," *J. Am. Chem. Soc.*, vol. 131, no. 17, pp. 6050–6051, May 2009, doi: 10.1021/ja809598r.

[10] A. M. Ganose, C. N. Savory, and D. O. Scanlon, "Beyond methylammonium lead iodide: prospects for the emergent field of ns 2 containing solar absorbers," *Chem. Commun.*, vol. 53, no. 1, pp. 20–44, 2017, doi: 10.1039/C6CC06475B.

[11] H.-H. Fang *et al.*, "Photophysics of Organic-Inorganic Hybrid Lead Iodide Perovskite Single Crystals," *Adv. Funct. Mater.*, vol. 25, no. 16, pp. 2378–2385, Apr. 2015, doi: 10.1002/adfm.201404421.

[12] R. Watanabe and H. Noji, "Timing of inorganic phosphate release modulates the catalytic activity of ATP-driven rotary motor protein," *Nat. Commun.*, vol. 5, no. 1, p. 3486, May 2014, doi: 10.1038/ncomms4486.

[13] A. Walsh, D. O. Scanlon, S. Chen, X. G. Gong, and S.-H. Wei, "Self-Regulation Mechanism for Charged Point Defects in Hybrid Halide Perovskites," *Angew. Chemie Int. Ed.*, vol. 54, no. 6, pp. 1791–1794, Feb. 2015, doi: 10.1002/anie.201409740.

[14] J. M. Frost, K. T. Butler, F. Brivio, C. H. Hendon, M. van Schilfgaarde, and A. Walsh,

"Atomistic Origins of High-Performance in Hybrid Halide Perovskite Solar Cells," *Nano Lett.*, vol. 14, no. 5, pp. 2584–2590, May 2014, doi: 10.1021/nl500390f.

[15] R. Lindblad *et al.*, "Electronic Structure of TiO 2 /CH 3 NH 3 PbI 3 Perovskite Solar Cell Interfaces," *J. Phys. Chem. Lett.*, vol. 5, no. 4, pp. 648–653, Feb. 2014, doi: 10.1021/jz402749f.

[16] Q. Lin, A. Armin, R. C. R. Nagiri, P. L. Burn, and P. Meredith, "Electro-optics of perovskite solar cells," *Nat. Photonics*, vol. 9, no. 2, pp. 106–112, Feb. 2015, doi: 10.1038/nphoton.2014.284.

[17] S. D. Stranks *et al.*, "Electron-Hole Diffusion Lengths Exceeding 1 Micrometer in an Organometal Trihalide Perovskite Absorber," *Science (80-.).*, vol. 342, no. 6156, pp. 341–344, Oct. 2013, doi: 10.1126/science.1243982.

[18] T. Hakamata, K. Shimamura, F. Shimojo, R. K. Kalia, A. Nakano, and P. Vashishta, "The nature of free-carrier transport in organometal halide perovskites," *Sci. Rep.*, vol. 6, no. 1, p. 19599, Apr. 2016, doi: 10.1038/srep19599.

[19] J. Even, L. Pedesseau, J.-M. Jancu, and C. Katan, "Importance of Spin–Orbit Coupling in Hybrid Organic/Inorganic Perovskites for Photovoltaic Applications," *J. Phys. Chem. Lett.*, vol. 4, no. 17, pp. 2999–3005, Sep. 2013, doi: 10.1021/jz401532q.

[20] S. D. Stranks and H. J. Snaith, "Metal-halide perovskites for photovoltaic and light-emitting devices," *Nat. Nanotechnol.*, vol. 10, no. 5, pp. 391–402, May 2015, doi: 10.1038/nnano.2015.90.

[21] C. Yu, "Advances in Modelling and Simulation of Halide Perovskites for Solar Cell Applications," *J. Phys. Energy*, p. 30, Nov. 2018, [Online]. Available: http://arxiv.org/abs/1811.00702.

[22] N. Soleimanioun, M. Rani, S. Sharma, A. Kumar, and S. K. Tripathi, "Binary metal zinc-lead perovskite built-in air ambient: Towards lead-less and stable perovskite materials," *Sol. Energy Mater. Sol. Cells*, vol. 191, no. June 2018, pp. 339–344, Mar. 2019, doi: 10.1016/j.solmat.2018.11.021.

[23] K. Wang, D. Yang, C. Wu, M. Sanghadasa, and S. Priya, "Recent progress in fundamental understanding of halide perovskite semiconductors," *Prog. Mater. Sci.*, p. 100580, Jul. 2019, doi: 10.1016/j.pmatsci.2019.100580.

[24] N. K. Noel *et al.*, "Lead-free organic–inorganic tin halide perovskites for photovoltaic applications," *Energy Environ. Sci.*, vol. 7, no. 9, pp. 3061–3068, 2014, doi: 10.1039/C4EE01076K.

[25] I. Kopacic *et al.*, "Enhanced Performance of Germanium Halide Perovskite Solar Cells through Compositional Engineering," *ACS Appl. Energy Mater.*, vol. 1, no. 2, pp. 343–347, Feb. 2018, doi: 10.1021/acsaem.8b00007.

[26] O. O. Johnson, P. E. Olutuase, and O. E. Oyewande, "First principles calculations of the optoelectronic properties of magnesium substitutes in Lead based ABX 3 compounds," *J. Phys. Conf. Ser.*, vol. 1299, p. 012129, Aug. 2019, doi: 10.1088/1742-6596/1299/1/012129.

[27] E. Meyer, D. Mutukwa, N. Zingwe, and R. Taziwa, "Lead-Free Halide Double Perovskites: A Review of the Structural, Optical, and Stability Properties as Well as Their

Viability to Replace Lead Halide Perovskites," *Metals (Basel).*, vol. 8, no. 9, p. 667, Aug. 2018, doi: 10.3390/met8090667.

[28] F. Igbari, Z. Wang, and L. Liao, "Progress of Lead- Free Halide Double Perovskites," *Adv. Energy Mater.*, vol. 9, no. 12, p. 1803150, Mar. 2019, doi: 10.1002/aenm.201803150.

[29] Z. Xiao, K. Du, W. Meng, J. Wang, D. B. Mitzi, and Y. Yan, "Intrinsic Instability of Cs 2 In(I)M(III)X 6 (M = Bi, Sb; X = Halogen) Double Perovskites: A Combined Density Functional Theory and Experimental Study," *J. Am. Chem. Soc.*, vol. 139, no. 17, pp. 6054–6057, May 2017, doi: 10.1021/jacs.7b02227.

[30] G. Volonakis *et al.*, "Cs 2 InAgCl 6 : A New Lead-Free Halide Double Perovskite with Direct Band Gap," *J. Phys. Chem. Lett.*, vol. 8, no. 4, pp. 772–778, Feb. 2017, doi: 10.1021/acs.jpclett.6b02682.

[31] J. Zhou, Z. Xia, M. S. Molokeev, X. Zhang, D. Peng, and Q. Liu, "Composition design, optical gap and stability investigations of lead-free halide double perovskite Cs 2 AgInCl 6," *J. Mater. Chem. A*, vol. 5, no. 29, pp. 15031–15037, 2017, doi: 10.1039/C7TA04690A.

[32] J. C. Dahl *et al.*, "Probing the Stability and Band Gaps of Cs 2 AgInCl 6 and Cs 2 AgSbCl 6 Lead-Free Double Perovskite Nanocrystals," *Chem. Mater.*, vol. 31, no. 9, pp. 3134–3143, May 2019, doi: 10.1021/acs.chemmater.8b04202.

[33] N. N. K. and A. Nag, "Synthesis and luminescence of Mn-doped Cs 2 AgInCl 6 double perovskites," *Chem. Commun.*, vol. 54, no. 41, pp. 5205–5208, 2018, doi: 10.1039/C8CC01982G.

[34] F. Liu *et al.*, "Ag/In lead- free double perovskites," *EcoMat*, vol. 2, no. 1, pp. 1–14, Mar. 2020, doi: 10.1002/eom2.12017.

[35] F. Locardi *et al.*, "Colloidal Synthesis of Double Perovskite Cs 2 AgInCl 6 and Mn-Doped Cs 2 AgInCl 6 Nanocrystals," *J. Am. Chem. Soc.*, vol. 140, no. 40, pp. 12989–12995, Oct. 2018, doi: 10.1021/jacs.8b07983.

[36] S. Yamanaka, K. Kurosaki, A. Charoenphakdee, H. Mastumoto, and H. Muta, "Thallium-Free Thermoelectric Materials with Extremely Low Thermal Conductivity," *MRS Proc.*, vol. 1044, pp. 1044-U08-02, Feb. 2007, doi: 10.1557/PROC-1044-U08-02.

[37] V. Kumar, K. Kumar, H. C. Jeon, T. W. Kang, D. Lee, and S. Kumar, "Effect of Cu-doping on the photoluminescence and photoconductivity of template synthesized CdS nanowires," *J. Phys. Chem. Solids*, vol. 124, pp. 1–6, Jan. 2019, doi: 10.1016/j.jpcs.2018.08.031.

[38] O. E. Oyewande and A. Akinpelu, "Projected Range and Sputter Yield of Ne + and Ar + in the Sputtering of Lead and Tin Perovskites," *IOP Conf. Ser. Earth Environ. Sci.*, vol. 173, no. 1, p. 012045, Jul. 2018, doi: 10.1088/1755-1315/173/1/012045.

[39] O. E. Oyewande, "A Unified Spatio-Temporal Framework of the Cuerno—Barabasi Stochastic Continuum Model of Surface Sputtering," *Commun. Theor. Phys.*, vol. 58, no. 1, pp. 165–170, Jul. 2012, doi: 10.1088/0253-6102/58/1/23.

[40] E. O. Yewande, R. Kree, and A. K. Hartmann, "Numerical analysis of quantum dots on off-normal incidence ion sputtered surfaces," *Phys. Rev. B*, vol. 75, no. 15, p. 155325, Apr. 2007, doi: 10.1103/PhysRevB.75.155325.

[41] O. El Rhazouani and A. Benyoussef, "Investigation by Monte Carlo simulation of substitution doping in the Double Perovskite Sr 2 CrRe 1−x W x O 6," *J. Magn. Magn. Mater.*, vol. 446, pp. 166–169, Jan. 2018, doi: 10.1016/j.jmmm.2017.09.015.

[42] E. O. Yewande, A. K. Hartmann, and R. Kree, "Propagation of ripples in Monte Carlo models of sputter-induced surface morphology," *Phys. Rev. B*, vol. 71, no. 19, p. 195405, May 2005, doi: 10.1103/PhysRevB.71.195405.

[43] N. J. Ramer and A. M. Rappe, "Virtual-crystal approximation that works: Locating a compositional phase boundary," *Phys. Rev. B - Condens. Matter Mater. Phys.*, vol. 62, no. 2, pp. R743–R746, 2000, doi: 10.1103/PhysRevB.62.R743.

[44] C.-J. Yu and H. Emmerich, "An efficient virtual crystal approximation that can be used to treat heterovalent atoms, applied to (1− x)BiScO 3 –x PbTiO 3," *J. Phys. Condens. Matter*, vol. 19, no. 30, p. 306203, Aug. 2007, doi: 10.1088/0953-8984/19/30/306203.

[45] N. . Ramer and A. . Rappe, "Application of a new virtual crystal approach for the study of disordered perovskites," *J. Phys. Chem. Solids*, vol. 61, no. 2, pp. 315–320, Feb. 2000, doi: 10.1016/S0022-3697(99)00300-5.

[46] P. Giannozzi *et al.*, "QUANTUM ESPRESSO: A modular and open-source software project for quantum simulations of materials," *J. Phys. Condens. Matter*, vol. 21, no. 39, 2009, doi: 10.1088/0953-8984/21/39/395502.

[47] P. Giannozzi *et al.*, "Advanced capabilities for materials modelling with Quantum ESPRESSO," *J. Phys. Condens. Matter*, vol. 29, no. 46, p. 465901, Nov. 2017, doi: 10.1088/1361-648X/aa8f79.

[48] J. P. Perdew, K. Burke, and M. Ernzerhof, "Generalized gradient approximation made simple," *Phys. Rev. Lett.*, vol. 77, no. 18, pp. 3865–3868, 1996, doi: 10.1103/PhysRevLett.77.3865.

[49] J. Klimeš, D. R. Bowler, and A. Michaelides, "Van der Waals density functionals applied to solids," *Phys. Rev. B*, vol. 83, no. 19, p. 195131, May 2011, doi: 10.1103/PhysRevB.83.195131.

[50] J. P. Perdew, M. Ernzerhof, and K. Burke, "Rationale for mixing exact exchange with density functional approximations," *J. Chem. Phys.*, vol. 105, no. 22, pp. 9982–9985, Dec. 1996, doi: 10.1063/1.472933.

[51] D. R. Hamann, "Optimized norm-conserving Vanderbilt pseudopotentials," *Phys. Rev. B*, vol. 88, no. 8, p. 085117, Aug. 2013, doi: 10.1103/PhysRevB.88.085117.

[52] H. J. Monkhorst and J. D. Pack, "Special points for Brillouin-zone integrations," *Phys. Rev. B*, vol. 13, no. 12, pp. 5188–5192, Jun. 1976, doi: 10.1103/PhysRevB.13.5188.

[53] F. Birch, "Finite Elastic Strain of Cubic Crystals," *Phys. Rev.*, vol. 71, no. 11, pp. 809–824, Jun. 1947, doi: 10.1103/PhysRev.71.809.